Structural Engineering and Mechanics, *Vol. 54, No. 1 (2015) 169-188*
DOI: http://dx.doi.org/10.12989/sem.2015.54.1.169

Seismic responses of base-isolated nuclear power plant structures considering spatially varying ground motions

Mohamed A. Sayed[1a], Sunghyuk Go[1b], Sung Gook Cho[2c] and Dookie Kim[*1]

[1]*Department of Civil and Environmental Engineering, Kunsan National University, South Korea*
[2]*INNOS TECH Company, Incheon, South Korea*

(Received March 4, 2014, Revised December 26, 2014, Accepted January 30, 2015)

Abstract. This study presents the effects of the spatial variation of ground motions in a hard rock site on the seismic responses of a base-isolated nuclear power plant (BI-NPP). Three structural models were studied for the BI-NPP supported by different number of lead rubber bearing (LRB) base isolators with different base mat dimensions. The seismic responses of the BI-NPP were analyzed and investigated under the uniform and spatial varying excitation of El Centro ground motion. In addition, the rotational degrees of freedom (DOFs) of the base mat nodes were taken to consider the flexural behavior of the base mat on the seismic responses under both uniform and spatial varying excitation. Finally, the seismic response results for all the analysis cases of the BI-NPP were investigated in terms of the vibration periods and mode shapes, lateral displacements, and base shear forces. The analysis results indicate that: (1) considering the flexural behavior of the base mat has a negligible effect on the lateral displacements of base isolators regardless of the number of the isolators or the type of excitation used; (2) considering the spatial variation of ground motions has a substantial influence on the lateral displacements of base isolators and the NPP stick model; (3) the ground motion spatial variation effect is more prominent on lateral displacements than base shear forces, particularly with increasing numbers of base isolators and neglecting flexural behavior of the base mat.

Keywords: base isolation; nuclear power plant; spatial variation; seismic analysis

1. Introduction

Base isolation also known as the seismic base isolation has been accepted as one of the most popular means of protecting a structure against severe earthquake forces (Datta 2010). Limited numbers of isolated structures have experienced significant earthquake shaking (Constantinou *et al*. 2007). Many researchers, e.g., (Stewart *et al*. 1999, Kani *et al*. 2006) investigated and reported that seismically isolated structures performed efficiently under earthquakes. Seismic isolation has been incorporated in the construction of significant numbers of conventional structures, bridges,

∗Corresponding author, Professor, E-mail: kim2kie@kunsan.ac.kr
[a]Researcher, E-mail: mabdelmonem86@gmail.com
[b]Researcher, E-mail: sunghyukgo@gmail.com
[c]CEO, E-mail: sgcho@innosetech.com

http://www.techno-press.org/?journal=sem&subpage=8 ISSN: 1225-4568 (Print), 1598-6217 (Online)

and infrastructures. However, to date, seismic isolation has only been applied to six nuclear reactors in two nuclear power plants (NPPs), which are located in France and South Africa (Malushte and Whittaker 2005, Huang *et al*. 2007, 2010). In addition, Forni (2011) cited a new nuclear reactor with a seismic base isolation system that is under construction in France. (Micheli *et al*. 2004, Zhao and Chen 2013) investigated the seismic responses of the NPP using base isolation devices under the seismic excitation. Forni *et al*. (2012) presented the state-of-the-art of the NPPs provided with seismic isolation along with rough recommendations on the design and construction of base-isolated nuclear power plants, since there is currently no specific standard for seismically isolated nuclear reactors or for isolators to be used in such plants to date.

The spatial variation of seismic ground motions indicates the differences and change in the amplitude and phase of seismic motions recorded over an extended area (Zerva and Zervas 2002). The spatial variation of ground motions causes can be summarized as; the wave passage effect, the extended source effect, the scattering effect and the attenuation effect (Zerva 2009). (Novak and Hindy 1979, Hindy and Novak 1980) were the pioneers that introduced the ground motions coherency losses as a mathematical description in the earthquake engineering field. Previous studies, e.g., (Zerva 1993, Der Kiureghian *et al*. 1997, Chakraborty and Basu 2008, Mwafy *et al*. 2011) integrated the spatial variation of seismic ground motions with extended structures, bridges and buried lifelines. In addition, other studies, e.g., (Luco and Wong 1986, Harichandran 1987, Kim and Stewart 2003) examined the response of rigid large mats and rigid foundations induced by spatially varying ground motions.

The NPP structures are designed under more severe regulations than general industrial and conventional structures. The seismic base isolation is a new challenge in the NPP industry. Potential problems should be carefully checked to adopt a new technology to the NPP. Many studies, e.g. (Hanamura *et al*. 1996, Ghiocel 2009, Nour *et al*. 2012) focused on investigating the seismic responses of the non-isolated NPPs considering the ground motions spatial variation. Nonetheless, very few studies have been conducted to study and examine the seismic responses of BI-NPPs considering spatially varying ground motions. It is necessary to investigate the effects of the spatial variation of ground motions on the responses of the BI-NPPs having large base mat. In addition, this study presented parametric results considering the effect of the spatial variation of ground motions on different base mat sizes of the BI-NPP.

The computer program SIMQKE-II developed by Vanmarcke *et al*. (1999) is used in this study to perform the conditional simulation of El Centro earthquake ground motion in a hard rock site, since the ideal NPP model is assumed to be connected and rested on a rock soil site. The basic inputs to the SIMQKE-II program are; the locations of the required simulated points, the power spectral density functions (PSDF) of the known recorded ground motions windows, the frequency-dependent spatial correlation function (to represent the coherency model between the known and simulated ground motions), and the known acceleration motion time history at the recording points. The SIMQKE-II program generates spatially correlated artificial ground motions based on Fast Fourier Transformation (FFT) compatible with PSDF of the reference (known) ground motion. The spatially varying ground motions in this study are assumed to have the same power spectrum density, since the site is assumed to be flat and with uniform soil properties. Bi and Hao (2012) illustrated that in flat and uniform soil sites, it is reasonable to assume that the spatially varying ground motion at various locations have the same power spectral density or response spectrum. Furthermore, a suggested scheme by Liao and Zerva (2006) which is based on the approach proposed by Boore *et al*. (2002) is used to extract the integrated displacement time histories from the conditionally simulated acceleration ground motions. These integrated

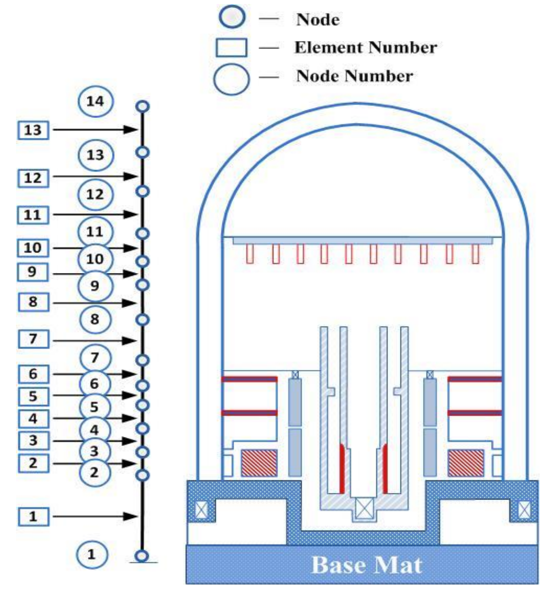

Fig. 1 NPP containment building sectional elevation and structural stick model

displacement time histories are used as multi-support (non-uniform) excitation on the NPP foundation mat nodes.

In this study, both the uniform and spatially varying multi-support excitation of El Centro ground motions are applied to the BI-NPP to investigate the seismic responses of the NPP. In addition, the rotational DOFs of the base mat nodes are considered to examine the flexural behavior of the base mat effect on the seismic responses of the BI-NPP under both uniform and multi-support excitation. Moreover, the influence of installing different numbers of the lead rubber bearing (LRB) isolators is investigated on the seismic responses of the BI-NPP. Three structural models of the BI-NPP are studied with the consideration of different numbers and properties of LRB isolators, and different dimensions of the base mat as well. In addition, the flexural behavior of the base mat is considered in all the analysis cases.

2. Base-Isolated NPP structural model

2.1 NPP stick model

The lumped mass stick model alongside with the hypothetical structural diagram of the nuclear power plant (NPP) reactor containment building (Lee and Song 1999) is represented in Fig. 1. The stick model of the NPP consists of fourteen nodes and thirteen elements with a total height of 65.8 m. The actual translational and rotational masses of the NPP are transferred as lumped masses to the corresponding nodes on each element’s edge.

2.2 Nuclear island base mat

Three structural models of the NPP containment building stick model and the nuclear island

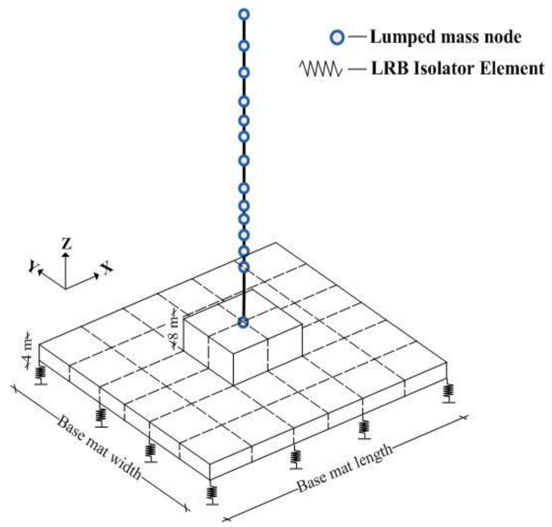

Fig. 2 Nuclear Island base mat dimensions

Table 1 BI-NPP models with different base mat dimensions

Model	Base mat dimensions			No. of LRB isolators		Total no. of isolators
	length (m)	width (m)	Area (m^2)	along *X*-dir.	along *Y*-dir.	
A	40	32	1280	5	5	25
B	60	48	2880	7	7	49
C	100	80	8000	11	11	121

base mat are established with different numbers and properties of LRB isolators and with different base mat dimensions as well. The BI-NPP numerical and analytical models were constructed in the OpenSees platform (McKenna and Fenves 2001) and compatible with OpenSees Navigator (Schellenberg *et al*. 2013). The three models with different LRB isolator numbers and base mat dimensions are presented in Table 1. The smallest base mat size (Model A) is selected to accommodate the reactor containment building dimensions. Fig. 2 illustrates the nuclear island base mat dimensions in the global axes, which is used complementarily with Table 1 to represent the three structural models of the BI-NPP.

2.3 Design of LRB isolators

The LRB base isolation device is composed of low damping natural rubber and a lead plug damper as shown in Fig. 3; where, the rubber is an elastic material. However, the lead plug damper becomes plastic at low levels of stress. Therefore, the LRB devices, as a whole, have very nonlinear dynamic properties. In this study, the LRB isolator was designed by adopting the design procedures and requirements of both the Japanese guidelines (JEA 2000) and the International Organization for Standardization (ISO) specifications (ISO 2010).

The isolator stiffness after the lead plug damper yielding is considered as the isolator key performance indicator. In this study, considering different base mat dimensions resulted in three total masses of the BI-NPP, which are 53,350 tons, 61,800 tons, and 110,950 tons for Model *A*, *B*,

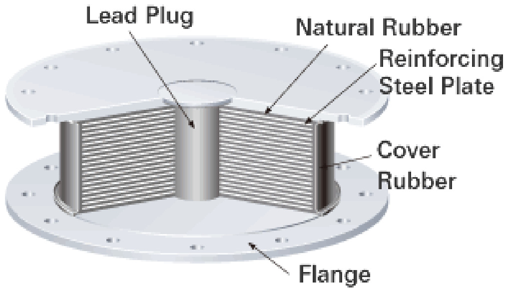

Fig. 3 Lead-plug rubber bearing

and *C*, respectively. The LRB dynamic properties of the three models of the BI-NPP are calculated and designed with considering the different base mat dimensions of the three models. Therefore, the LRB isolator properties are redesigned for the three models considering different total mass and weight of the structure in the three models. Therefore, after the lead damper yielding, the isolators' horizontal stiffness for each model is presented by the following equation

$$K_{total} = M\left(\frac{2\pi}{T_H}\right)^2 \tag{1}$$

Where, K_{total} is the total global horizontal tangential stiffness of the system; M is the total mass of the isolated structure; T_H is the target natural period of vibration of the isolated structure which was preliminary set as 2 sec. Subsequently, the horizontal stiffness of a single isolator in every model is calculated by

$$K_H = \frac{K_{total}}{N} \tag{2}$$

Where, K_H is the horizontal (effective) tangential stiffness of the single isolator; and N is the number of isolators in every model, which are 25, 49, 121 for Model *A*, *B*, and *C*, respectively. Fig. 4 shows the bilinear model of the dynamic properties of the LRB isolator. The linear (unloading) horizontal stiffness of the isolator before the lead plug yielding K_u=(4~6.5)*K_H and it is taken as K_u=4*K_H; while, the yield strength F_y=(3~5%)*W, where W is the total weight of the NPP and it is taken as F_y=5% W (JEA 2000). Moreover, the characteristic strength of the isolator is calculated by

$$Q_d = F_y\left(1 - \frac{K_H}{K_u}\right) \tag{3}$$

The design horizontal displacement of the isolator device δ_0 is assumed to be 200 mm, and by considering a factor of safety, the maximum horizontal displacement at break δ_b=350 mm. The total thickness of the laminated rubber layers of the isolator is calculated using $T_r=(\delta_b/\gamma_b)$, where γ_b is the maximum horizontal strain at break which is assumed 2. Therefore, the first estimation of the total thickness of the rubber layers is calculated as 175 mm. In addition, the number of laminated rubber layers can be represented as $n=(T_r/t_r)$; where, T_r the total thickness of the laminated rubber, and t_r is a single rubber layer thickness.

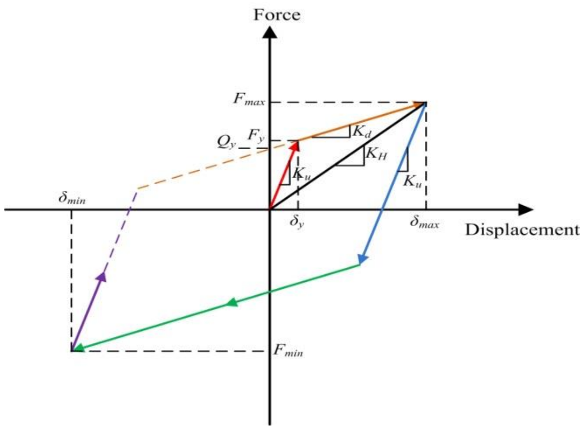

Fig. 4 Linearization of force-displacement relationship of LRB isolator

The design horizontal strain of the laminated rubber material γ_0=(δ_0/T_r); while the equivalent linear shear modulus of the rubber layers is calculated as follows (ISO 2010)

$$G_{eq}(\gamma_0) = 6.067 - 1.437\gamma_0 + 0.4653\gamma_0^{\ 2} \tag{4}$$

The shear modulus of the lead plug bar

$$G_p(\gamma_0) = \begin{cases} 170(1-\gamma_0)^3 & \gamma_0 < 1 \\ 0 & \gamma_0 \geq 1 \end{cases} \tag{5}$$

The yield stress of the lead plug

$$\tau_p(\gamma_0) = 38 + 102\gamma_0 - 68\gamma_0^{\ 2} + 15\gamma_0^{\ 3} \tag{6}$$

The lead plug bar cross sectional area

$$A_p = \frac{Q_d}{\tau_p(\gamma_0)} \tag{7}$$

The effective cross sectional area of the rubber layers excluding the cover rubber portion

$$A = (K_H - \frac{A_p G_p(\gamma_0)}{T_r}) * (\frac{T_r}{G_{eq}(\gamma_0)}) \tag{8}$$

The post-yield horizontal stiffness of the isolator after yielding of the lead plug bar

$$K_d = K_H - \frac{Q_d}{\gamma_0 T_r} \tag{9}$$

The yield displacement

$$\delta_y = \frac{Q_d}{K_u - K_d} \tag{10}$$

Table 2 Properties of the LRB base isolation device

Model	Horizontal Stiffness	Post-yielding Stiffness	Yield Strength	Characteristic Strength	Yield Displacement
	K_H (KN/m)	K_d (KN/m)	F_y (KN)	Q_d (KN)	δ_y (mm)
A	19956.95	16631.79	748.72	665.03	5.03
B	11733.64	9825.26	430.13	381.67	4.93
C	8436.10	7089.54	303.73	269.31	4.85

Table 3 LRB base isolator device components dimension

Model	Total no. of isolators	no. of rubber layers	rubber layer thickness (mm)	Total thickness of the rubber layers (mm)	Total thickness of the isolator (mm)	Lead plug diameter (mm)	Outer diameter of isolator (mm)
A	25	10	18	180	350	330	3000
B	49	10	18	180	350	250	2300
C	121	10	18	180	350	210	1950

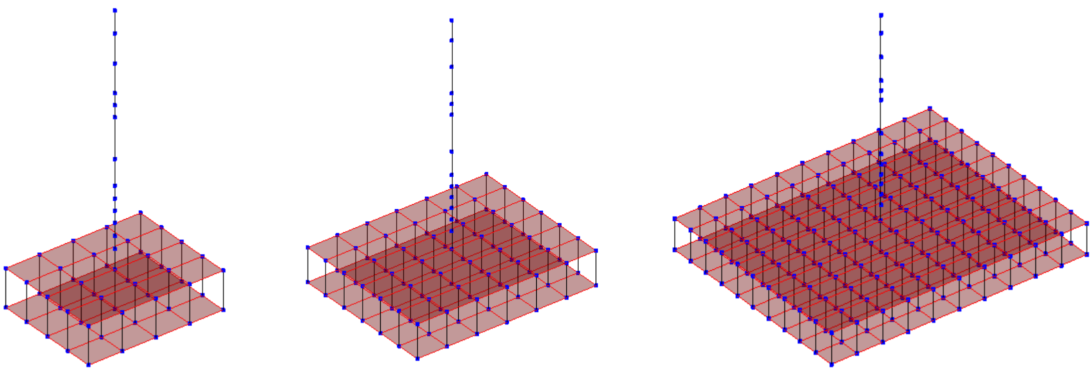

(a) Model A (b) Model B (c) Model C

Fig. 5 BI-NPP structural models with different base mat dimensions and LRB isolator numbers

Table 2 illustrates the dynamic properties of the designed LRB isolators for the three models, which are used in this study to investigate the seismic responses of the BI-NPP. Moreover, Table 3 demonstrates the LRB isolator components dimension for the three models of the BI-NPP. Fig. 5 illustrates the structural models of the three BI-NPP models; i.e., Model *A*, *B*, and *C*.

For each of the three models, the rotational DOFs of base mat nodes about the longitudinal and transverse directions (*X*- and *Y*-direction) are allowed to consider and examine the base mat's flexural behavior effect on the seismic responses of the BI-NPP. The nuclear island base mat's thicknesses are 12 m under the NPP stick model with dimensions (20 m×16 m), and 4 m thickness for the rest of base mat area for all the three models. Therefore, the soil structure interaction was not considered in this study since the BI-NPP is based on a thick foundation and rested on a rock site. In addition, proper boundary conditions are assigned for the nuclear island lower foundation.

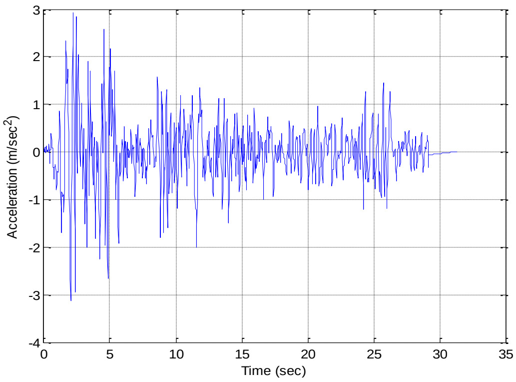

Fig. 6 El Centro acceleration time history

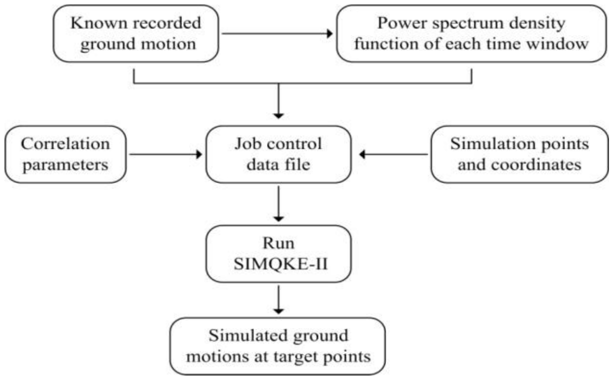

Fig. 7 SIMQKE-II procedure steps to simulate spatially correlated earthquake ground motions

3. The spatial variation of ground motions

3.1 El Centro ground motion

For studying the effect of the spatial variation of ground motions on the seismic responses of the BI-NPP and the time history analysis, the 1940 El Centro earthquake is studied and considered as the recorded known (reference) time history. El Centro earthquake is considered the first major earthquake to be recorded by a strong-motion seismograph that was located next to a fault rupture. In addition, it is often used in analysis of structures, particularly for the time history analysis method. Previous studies, e.g., (Tongaonkar and Jangid 2003, Soneji and Jangid 2008) have considered El Centro earthquake regarding the seismic analysis of base-isolated bridges and structures considering different soil types ranging from soft, medium, hard, and rock soil conditions. Therefore, in this study, the recorded El Centro time history is used to generate the correlated conditionally simulated ground motions at target distances, with spacing 10 m, considering the spatial variation of ground motion. Fig. 6 illustrates the acceleration time history of the El Centro earthquake with a time increment of 0.02 sec and peak ground acceleration (PGA) of 0.32 g.

The computer program SIMQKE-II developed by Vanmarcke *et al*. (1999) is used to perform the conditional simulation of the referenced El Centro ground motion. In the conditional simulation, the simulated ground motions are statically compatible with, or conditioned by, the recorded known ground motion. The basic inputs to the SIMQKE-II program are; the locations of the required simulated points, the spectral density functions of the known recorded ground motions windows, the frequency-dependent spatial correlation function, and the known ground motion time history at the recording points. Fig. 7 illustrates the SIMQKE-II procedure steps for simulating spatially correlated earthquake ground motions at required distances; where, the reference El-Centro ground motion is subdivided into a sequence of successive time windows, wherein the PSDF for each time window is calculated. In addition, in this study, the El Centro spatially varying ground motions are assumed to have the same power spectrum density since the site is assumed to be flat and with uniform soil properties.

3.2 Coherency model

The following isotropic frequency-dependent spatial correlation function provided by Vanmarcke *et al*. (1999) is used in compatibility with the SIMQKE-II program to perform the conditional simulation of the El Centro's reference (known) ground motion

$$\rho_{\omega k}(r_{ij}) = \exp\left\{\frac{-\omega_k |r_{ij}|}{2\pi c s}\right\} \tag{11}$$

Where, r_{ij} is the relative position vector between the recorded and simulated ground motions, c is the shear wave velocity of the soil medium, and s is the distance-scale parameter. Through changing the distances between the recorded and simulated ground motions while fixing the distance-scale parameter value, the degree of correlation can be controlled. In this study, the spatial variation of ground motion is considered to be simulated in a hard rock site; since the ideal NPP model is assumed to be connected and rested on a rock soil site. Therefore, the shear wave velocity is assumed 2500 m/sec, which is considered an acceptable assumption for neglecting the soil structure interaction (USNRC 2012). The selected site with 2500 m/sec shear wave velocity is considered as a hard rock site according to the ASCE 7-10 (2010). Moreover, the distance-scale parameter value was assumed 5 based on a previous study by Vanmarcke *et al*. (2003). Thus, assuming the distance-scale parameter value to be 5 refers to a high correlation between the known and simulated ground motions and makes the simulated motion at a distance of 10 m look fairly similar to the recorded ground motion (Vanmarcke *et al*. 1999). The relatively high correlation is assumed between the known and simulated ground motions due to the relatively small simulation target distances among the simulated ground motions. Where, the simulated ground motions were performed using simulation distances with 10 m spacing with a total simulation distance of 100 m, which represents the largest length in the longitudinal direction (*X*-direction) of the nuclear base mat in Model *C*.

3.3 Conditionally simulated ground motions

Fig. 8(a) shows the reference El Centro ground motion at (r=0 m) and the conditionally simulated ground motions in the uniform hard rock site with shear wave velocity of 2500 m/sec at distances of 50 m and 100 m, respectively. The simulated ground motions at 50 m and 100 m show relatively high correlation with the known ground motions as expected, due to assuming the

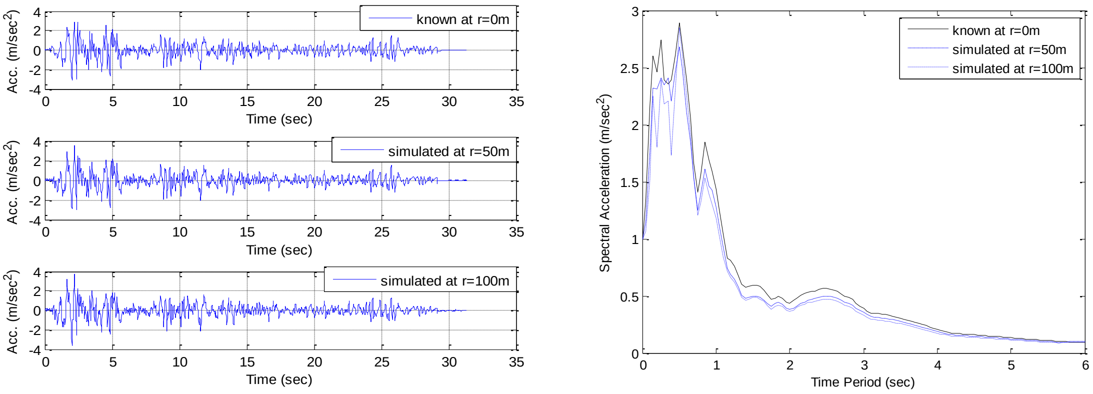

(a) Acceleration time histories of the known and simulated ground motions

(b) Acceleration response spectra at 5% damping

Fig. 8 El Centro known and conditionally simulated ground motions at distances of 50 m and 100 m

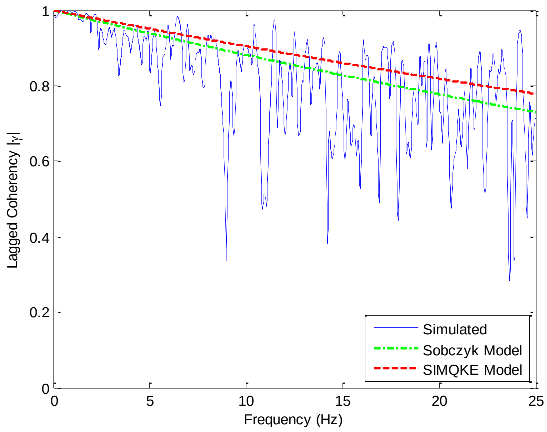

Fig. 9 Comparison of coherency loss between simulated ground motions at 100 m with model coherency loss functions

distance-scale parameter value to be 5, which refers to a high correlation between the known and simulated ground motions. In addition, Fig. 8(b) illustrates the acceleration response spectra of the known and simulated ground motions at 5% damping.

SIMQKE model and the Sobczyk model (Sobczyk 1991, Bi and Hao 2012) are selected to investigate the coherency loss between the reference and simulated ground motions. Fig. 9 illustrates the coherency loss functions of the simulated ground motion at 100 m, and the prescribed models. Good matching between the models and the simulated coherency loss functions is observed.

3.4 Integrated displacement time histories

After generating the correlated conditionally simulated ground motions using SIMQKE-II software at the target locations for rock site conditions with 10 m spacing, a suggested processing scheme for simulation and conditional simulation by Liao and Zerva (2006) is used to extract the displacement time histories from simulated artificial acceleration histories. In the suggested scheme, the high-pass filter is applied to the acceleration time histories, followed by double integration of the acceleration to extract the displacement time histories. These integrated displacement time histories are used as multi-support excitation at the BI-NPP foundation mat nodes at the different target distances along the longitudinal direction (*X*-direction) of the BI-NPP.

The most commonly used filter, by the US Geological Survey (USGS) and the Pacific Earthquake Engineering Research Center (PEER) is the Butterworth filter (Zerva 2009). Therefore, the Butterworth high-pass filter is applied in this study to extract the displacement time histories from the known and simulated ground motions. The most critical point in applying the Butterworth high-pass filter is selecting the filter order and the filter corner frequency. Following the approach by Boore *et al*. (2002), a 4-th order Butterworth high-pass filter is applied. Liao and Zerva (2006) proposed a purely numerical criterion to evaluate the corner frequency for the selected filter, which can be calculated as

$$fc = \frac{1}{T\left[\frac{H_0^2}{(1-H_0^2)}\right]^{\frac{1}{2n}}} \tag{12}$$

Where, f_c is the corner frequency, n is the high-pass filter order, T is the ground motion time and H_0 is the filter amplitude threshold. Liao and Zerva (2006) suggested that the amplitude threshold to be selected as H_0=0.02, which implies that at least 98% of the low frequency components with a period longer than the ground motions time history duration are filtered out. Therefore, the calculated corner frequency from Eq. (12) with the 4-th order Butterworth high-pass filter is applied to extract the integrated displacement time histories from the reference and simulated ground motions. Fig. 10 represents the integrated displacement time histories for the reference recorded El Centro ground motion at (r=0 m) and the simulated time history at 50 m and 100 m, respectively. In Fig. 10, a relatively high correlation between the integrated displacement time histories is noticed as a result of the relatively high correlation between the known and simulated acceleration ground motions.

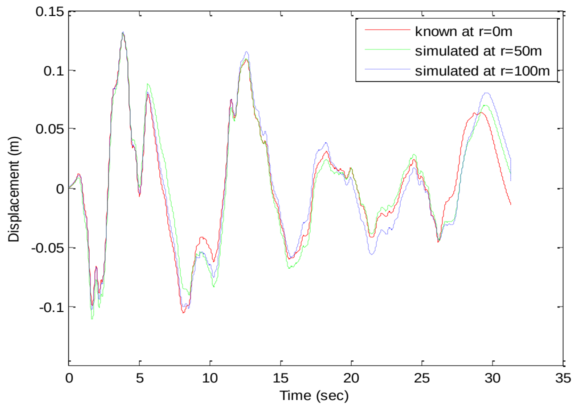

Fig. 10 El Centro known and simulated integrated displacement time histories at 50 m and 100 m

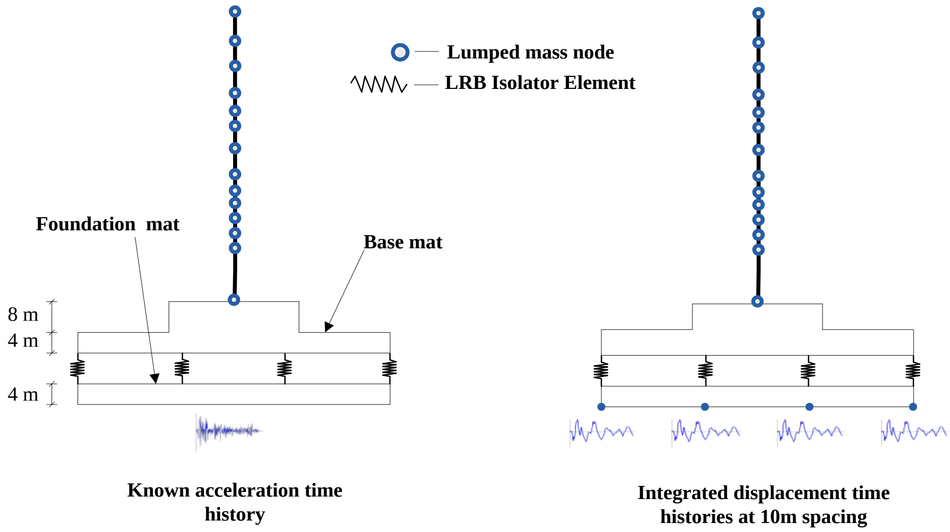

(a) Uniform excitation (b) Multi-support excitation

Fig. 11 Uniform and multi-support excitation on the BI-NPP

4. Results and discussions

The reference and simulated El Centro ground motions are applied along the longitudinal direction (X-direction) of the BI-NPP in two excitation types; i.e., uniform and multi-support excitation analysis. In the uniform excitation case, only the known acceleration time history is applied to the BI-NPP structural models as a uniform ground motion input. However, in the multi-support excitation case, the integrated displacement time histories from the simulated ground motions considering the ground motion spatial variation at different distances are applied to the foundation mat nodes. Both the uniform and multi-support excitation schemes are shown in Fig. 11. Furthermore, both uniform and multi-support excitation are applied to the three models of the BI-NPP considering different base mat dimensions and numbers of LRB isolators.

Moreover, two analysis conditions are considering of all the three models; i.e., preventing the rotational DOFs of the base mat nodes to examine the base mat's rigid behavior, and allowing the rotational DOFs of the base mat about X- and Y- direction. The rotational DOFs of base mat are allowed to consider the flexural behavior effect of the base mat on seismic responses. The seismic response results of each model and analysis case are investigated in terms of the modal analysis, and earthquake analysis; the results are presented in the next section.

4.1 Modal analysis

The modal analysis is applied to all the BI-NPP three models after designing the base isolators to a target fundamental period of 2 sec as described in Eq. (1). Fig. 12 illustrates the first mode shapes and periods of the BI-NPP for Model C. It considers the rotational DOFs of the base mat nodes and compares it to the one that does not consider rotational DOFs of the base mat.

Considering the flexural behavior of the base mat through allowing the base mat nodes rotational DOFs increased of the first natural period from 2.06 sec to 2.08 sec as presented in Fig.

Table 4 Fundamental periods of the three models of BI-NPP

Case	Fundamental natural period (sec)		Increase (%)
	w/o ROT DOFs of base mat	with ROT DOFs of base mat	
Model A: 25-isolators	2.03	2.06	1.47
Model B: 49-isolators	2.04	2.07	1.41
Model C: 121-isolators	2.06	2.08	0.97

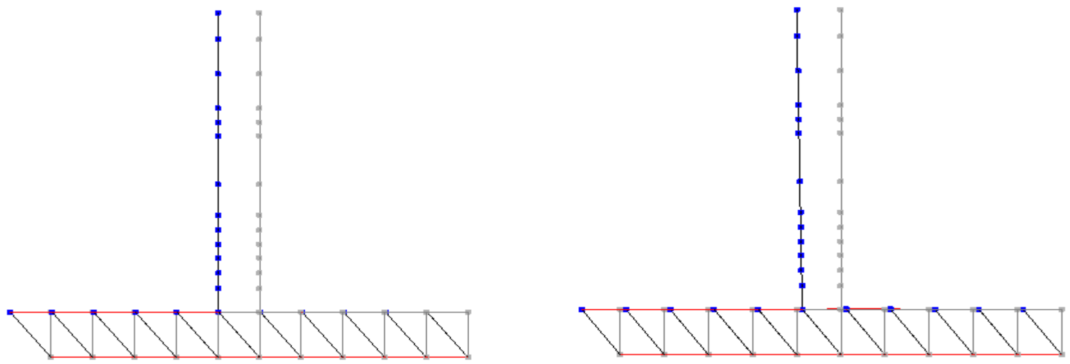

(a) Model *C* without considering the rotational DOFs of base mat nodes, T_1=2.06 sec

(b) Model *C* with considering the rotational DOFs of base mat nodes, T_1=2.08 sec

Fig. 12 First mode shapes and fundamental periods of Model *C* of the BI-NPP with considering of 121 LRB base isolators

12. Table 4 represents the first natural period of all three models of the BI-NPP; in addition to the effect of considering the flexural behavior of base mat on the fundamental period. The modal analysis results demonstrate that allowing the rotational DOFs of base mat nodes, i.e., considering the flexural behavior of the base mat, increased the first natural period of the BI-NPP by 1.47%, 1.41% and 0.97% with considering of 25, 49 and 121 isolators for Model *A*, *B*, and *C*, respectively.

4.2 Earthquake analysis

4.2.1 Lateral displacement

Fig. 13 and Table 5 illustrate the maximum horizontal lateral displacements, in meters, of the base isolators and the NPP stick model top node under the uniform and spatially varying multi-support excitation of the El Centro ground motions for the three models of the BI-NPP. These results are for both cases: considering and neglecting the flexure of the base mat, i.e., the base mat nodes' rotational DOFs. The lateral displacements of the base isolators for the three models are below the allowable base isolator design displacement.

It can be shown through Table 5 and Fig. 13, that considering the flexural behavior of the base mat by allowing the rotational DOFs of base mat nodes has a minor effect on the base isolators lateral displacements; whereas, considering the base mat's flexural behavior changed the base isolation lateral displacement by 1.4%, 0.3%, and 1.9% under the uniform excitation, while it modified the base isolation lateral displacement by 3.1%, 0.4%, and 0.9% under the spatially varying multi-support excitation for Model *A*, *B* and *C*, respectively. However, considering the flexural behavior of the base mat has more significant influence on the NPP stick model top node

Table 5 Maximum lateral displacements of LRB isolators and NPP stick model top node for the three models under uniform and multi-support excitation

Model	with base mat rotational DOFs				w/o base mat rotational DOFs			
	Uniform		Multi-support		Uniform		Multi-support	
	Base isolators	NPP top node	Base isolators	NPP top node	Base isolators	NPP top node	Base isolators	NPP top node
A	0.1385	0.1482	0.1486	0.1554	0.1404	0.1411	0.1442	0.1449
B	0.1354	0.1454	0.1502	0.1579	0.1350	0.1356	0.1496	0.1506
C	0.1272	0.1394	0.1427	0.1464	0.1297	0.1302	0.1439	0.1446

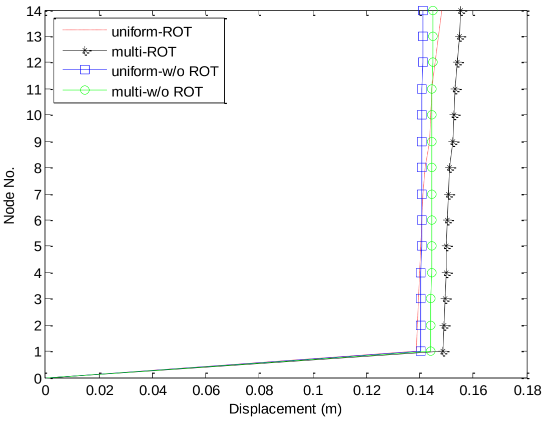

(a) Model A

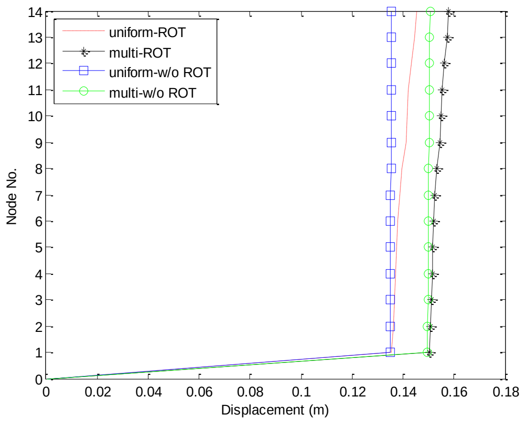

(b) Model B

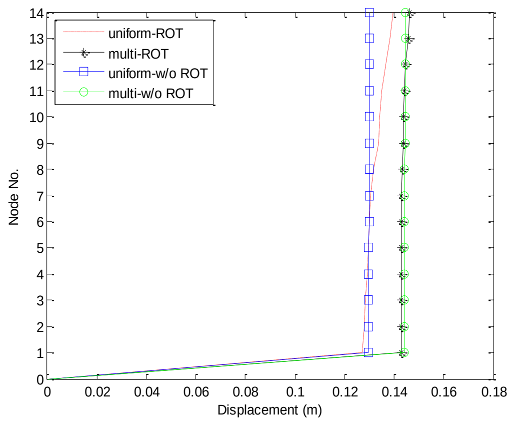

(c) Model C

Fig. 13 Maximum lateral displacement of the BI-NPP under uniform and multi-support excitation with and without considering the base mat rotational DOFs

lateral displacement; as it increased the NPP stick model top node lateral displacement by 5.0%, 7.3%, and 7.1% under the uniform excitation and by 7.2%, 4.9%, and 1.2% under the spatially varying multi-support excitation for Model *A*, *B*, and *C*, respectively.

Investigating the influence of the spatially varying multi-support excitation on the lateral

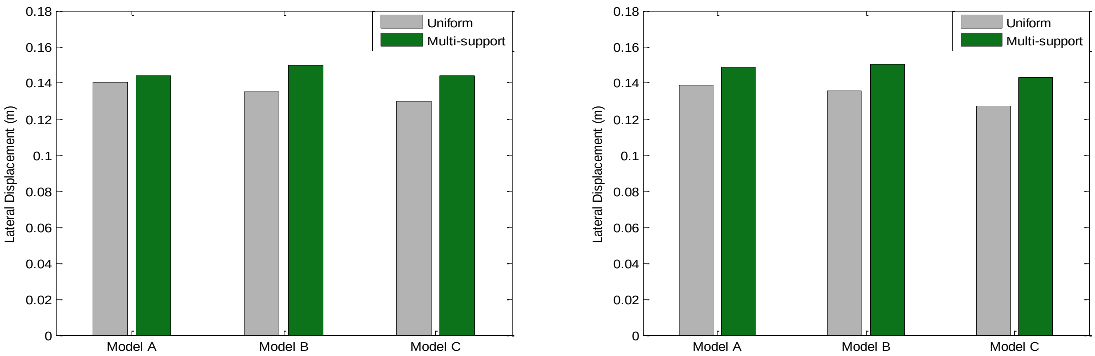

(a) without considering base mat rotational DOFs (b) with considering base mat rotational DOFs

Fig. 14 Maximum lateral displacements of the base isolators under uniform and multi-support excitation

displacement of base isolators shows a significant and an increasing effect when increasing the number of isolators (and thus increasing the base mat dimension) as shown in Fig. 14. Whereas, applying the spatially varying multi-support excitation comparable to the uniform excitation increased the base isolators lateral displacement by 7.3%, 11.0%, and 12.1% with considering the flexural behavior of the base mat; while, it increased the lateral displacement of base isolators by 2.7%, 10.9%, and 11.0% with neglecting the base mat's flexural behavior for Model *A*, *B*, and *C*, respectively. Similarly, considering the spatially varying multi-support excitation follows the same pattern on the NPP stick model lateral displacement as shown in Fig. 13. Where, applying the spatially varying multi-support excitation increased the lateral displacement of the NPP stick model top node by 4.8%, 8.6%, and 5.0% when considering the base mat's flexure behavior; while, it increased the NPP stick model top node lateral displacement by 2.7%, 11.1%, and 11.1% when neglecting the flexural behavior of the base mat for case A, B, and C, respectively.

Finally, it can be noticed that the inter-story drift (the NPP stick model top node's lateral displacement minus the base isolators' later displacement) resulted in a higher increase under the uniform excitation than under the multi-support excitation, particularly with considering the flexural behavior of the base mat. Where, the inter-story drift was 9.70 mm, 10.01 mm, and 12.18 mm under the uniform excitation; however, it was 6.72 mm, 7.71 mm, and 3.69 mm under the multi-support excitation for Model *A*, *B*, and *C*, respectively, with considering the bas mat flexural behavior. Conversely, the NPP inter-story drift values dropped dramatically when preventing the flexural behavior of the base mat under uniform and multi-support excitation. Whereas, the inter-story drift became 0.68 mm, 0.59 mm, 0.55 mm under the uniform excitation and 0.71 mm, 0.93 mm, and 0.70 mm under the spatially varying multi-support excitation for Model *A*, *B*, and *C*, respectively, as shown in Fig. 13. The inter-story drift results indicate that with the consideration of the flexural behavior of the base mat, the inter-story drift shows higher values under the uniform excitation; however, the inter-story drift tends to be larger under the spatially varying multi-support than the uniform excitation with neglecting the bas mat flexural behavior.

4.2.2 Base shear

Fig. 15 demonstrates the maximum shear forces along the NPP stick model under both uniform and spatially varying multi-support excitation of the El Centro ground motions when considering the rotational DOFs of the base mat nodes for three different models of the BI-NPP.

Fig. 15(a) shows that, for Model *A* with 25-isolators, considering the base mat nodes' rotational DOFs increased the maximum base shear of the NPP by 84.2% under uniform excitation; while, it increased the base shear by 36.3% under spatially varying multi-support excitation. Similarly, when the increasing the number of isolators in Model *B*, in Fig. 15(b), a significant increase in base shear forces due to considering the base mat's rotational DOFs is noticed under uniform and multi-support excitation; where, considering the rotational DOFs increased the base shear by 46.3% and 34.1% under uniform and spatially varying multi-support excitation, respectively, for Model *B*. In addition, when increasing the number of isolators and consequently the base mat dimensions in Model *C* with 121-isolators, Fig. 15(c) shows a similarity with Model *A* and *B*, where considering the rotational DOFs of the base mat nodes increased the maximum base shear significantly by 86.6% and 111.8% under uniform and spatially varying multi-support excitation, respectively, for Model *C*.

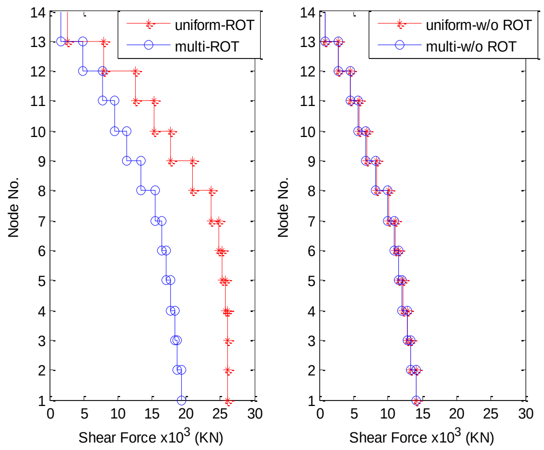

(a) Model A

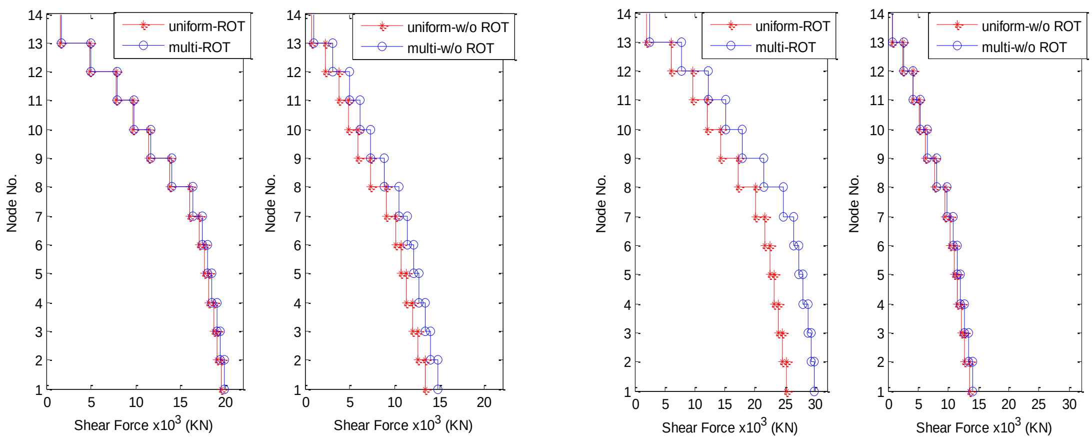

(b) Model B (c) Model C

Fig. 15 Maximum shear forces along the NPP stick model under uniform and multi-support excitation with and without considering base mat nodes rotational DOFs

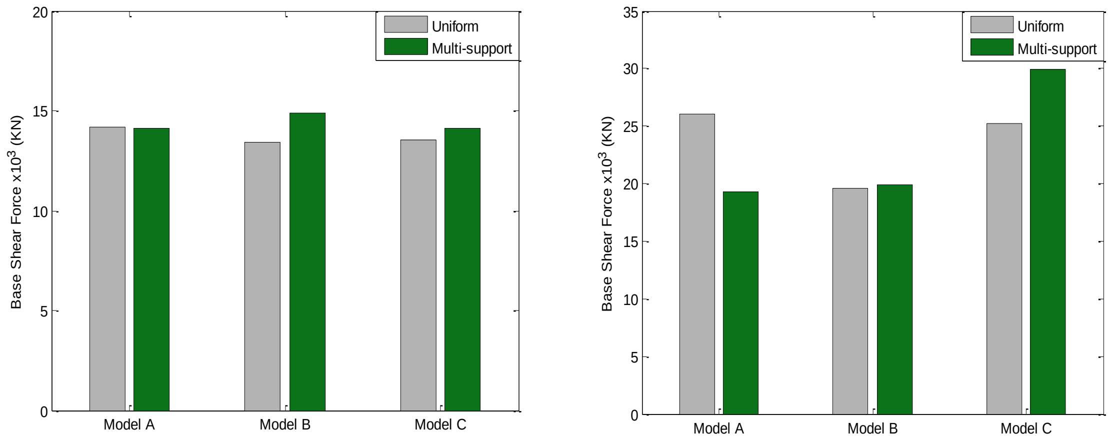

(a) without considering base mat rotational DOFs (b) with considering base mat rotational DOFs

Fig. 16 Maximum base shear forces of the BI-NPP under uniform and multi-support excitation

Further, examining the effect of the spatial variation of ground motions represented in the multi-support excitation has a noticeable influence in the base shear values for all three models as shown in Fig. 16. Where, the effect of the multi-support excitation compared to the uniform excitation decreased the maximum base shear of the NPP stick model by 26% and 0.1% with considering the rotational DOFs of the base mat and neglecting it, respectively, for Model A. However, by increasing the number of isolators and base mat dimensions in Model B, the effect of the multi-support excitation increased the maximum base shear by 1.7% and 11.0% when considering the rotational DOFs of the base mat and neglecting it, respectively. Finally, in Model C, the ground motion spatial variation increased the maximum shear force by 18.6% and 4.5% when considering the base mat's rotational DOFs and neglecting it, respectively. These spatial varying multi-support results show that with the prevention of the base mat flexural behavior the maximum base shear suffered a slight increase with increasing the base mat dimensions and hence increasing the number of isolators. Conversely, the multi-support excitation had a sever effect on maximum base shear forces with the considering the flexural behavior of the base mat and with increasing the base mat dimensions as shown in Fig. 16.

5. Conclusions

The current study reports the seismic responses of three models of the BI-NPP supported by 25, 49, and 121 LRB base isolators. In addition, the spatial variation of the El Centro ground motion in a hard rock site was investigated and applied as a multi-support excitation on the BI-NPP base mat. In addition, the seismic responses of the BI-NPP are investigated under both uniform and spatial varying multi-support excitation of El Centro ground motion. Moreover, the rotational DOFs of base mat nodes are allowed to consider and examine the flexure behavior of the base mat effect on the seismic responses. The conclusions drawn from this study are as follow:

• The modal analysis results demonstrate that, considering the flexural behavior of the base mat increases the fundamental natural period of the BI-NPP. Therefore, the rocking motion effect of the base mat becomes more noticeable after considering the rotational DOFs. However, considering the base mat's flexural behavior shows a decreasing influence with increasing the base mat dimensions, and thus increasing the number of base isolators.

• Regardless of the number of base isolators or the type of excitation used, the lateral displacements of the base isolators for the three models are below the allowable base isolator design displacement.

• Considering the flexure behavior of the base mat by allowing the base mat nodes rotational DOFs has a minor or negligible effect on the base isolators lateral displacements regardless of the number of base isolators or the type of excitation used. However, considering the base mat flexural behavior has a more significant influence on the NPP stick model inter-story drift and top node lateral displacement, particularly under the uniform excitation. Moreover, it has a significant effect when increasing the number of isolators on the NPP base shear forces under spatially varying multi-support excitation.

• Considering the spatial variation of ground motions has a significant and an increasing effect on the base isolator later displacements with increasing the number of isolators and hence increasing the base mat dimensions. However, with increasing the base mat dimensions the NPP stick model inter-story drift suffered a higher increase under the uniform excitation than under the multi-support excitation.

• Considering the spatial variation of ground motions shows a minor increase on the maximum base shear forces with increasing the base mat dimensions and neglecting flexural behavior of the base mat. Conversely, the multi-support excitation has a sever effect on the maximum base shear forces with considering the flexural behavior of the base mat and with increasing the base mat dimensions.

• Finally, the results of BI-NPP seismic responses indicate that the effect of the ground motion spatial variation is more prominent on the lateral displacements than shear forces, particularly with increasing the number of base isolators (increasing the base mat dimensions) and neglecting the base mat's flexural behavior.

Acknowledgments

This work was supported by the Nuclear Power Core Technology Development Program of the Korea Institute of Energy Technology Evaluation and Planning (KETEP) grant financial resource from the Ministry of Trade, Industry & Energy, Republic of Korea (No. 2011151010010A).

References

American Society of Civil Engineers (ASCE) (2010), *Minimum design loads for buildings and other structures*, ASCE/SEI 7-10, ASCE, Reston, VA.

Bi, K. and Hao, H. (2012), "Modeling and simulation of spatially varying earthquake ground motions at sites with varying conditions", *Probab. Eng. Mech.*, **29**, 92-104.

Boore, D.M., Stephens, C.D. and Joyner, W.B. (2002), "Comments on baseline correction of digital strong motion data: Examples of the 1999 Hector Mine, California, Earthquake", *Bul. Seismol. Soc. Am.*, **92**, 1543-1560.

Chakraborty, A. and Basu, B. (2008), "Nonstationary response analysis of long span bridges under spatially varying differential support motions using continuous wavelet transform", *J. Eng. Mech.*, ASCE, **134**(2), 155-162.

Constantinou, M.C., Whittaker, A.S., Kalpakidis, Y., Fenz, D.M. and Warn, G.P. (2007), "Performance of seismic isolation hardware under service and seismic loading", Technical Report MCEER-07-0012, Multidisciplinary Center for Earthquake Engineering Research, State University of New York, Buffalo, New York, USA.

Datta, T.K. (2010), *Seismic Analysis of Structures*, John Wiley & Sons (Asia), Singapore.

Der Kiureghian, A., Keshishian, P. and Hakobian, A. (1997), "Multiple support response spectrum analysis of bridges including the site response effect and the MSRS code", Earthquake Engineering Research Center Report No. UCB/EERC-97/02, University of California, Berkeley, CA, USA.

Forni, M. (2011), "Seismic isolation of nuclear power plants", *Contribution to the "Italy in Japan 2011" Initiative Science*, Technology and Innovation, 1-8.

Forni, M., Poggianti, A. and Dusi, A. (2012), "Seismic isolation of nuclear power plants", *Proceedings of the 15th World Conference of Earthquake Engineering*, Paper no. 1485, Lisbon, Portugal, September.

Ghiocel, D.M. (2009), "Seismic motion incoherency effects on soil structure interaction (SSI) response of nuclear power plant buildings", *Proceedings of the 10th International Conference in Structural Safety and Reliability*, ICOSSAR 2009, Osaka, Japan, September.

Hanamura, M., Suhara, J., Takada, T., Ogo, H. and Ichihashi, I. (1996), "Influence of spatial variation of earthquake ground motion on the response of secondary systems", *Proceedings of the 11th World Conference on Earthquake Engineering*, Paper no. 1296, Acapulco, Mexico, June.

Harichandran, R.S. (1987), "Stochastic analysis of rigid foundation filtering", *Earthq. Eng. Struct. Dyn.*, **15**, 889-899.

Hindy, A. and Novak, M. (1980), "Pipeline response to random ground motion", *J. Eng. Mech. Div.*, ASCE, **106**, 339-360.

Huang, Y.N., Whittaker, A.S., Constantinou, M.C. and Malushte, S. (2007), "Seismic demands on secondary systems in base-isolated nuclear power plants", *Earthq. Eng. Struct. Dyn.*, **36**, 1741-1761.

Huang, Y.N., Whittaker, A.S. and Luco, N. (2010), "Seismic performance assessment of base-isolated safety-related nuclear structures", *Earthq. Eng. Struct. Dyn.*, **39**, 1421-1442.

Kani, N., Takayama, M. and Wada, A. (2006), "Performance of seismically isolated buildings in Japan", *Proceedings of the 8th US National Conference of Earthquake Engineering*, Paper no. 2181, San Francisco, CA, USA, April.

International Standard Organization (ISO) (2010), *Elastomeric Seismic-Protection Isolators-Part 3: Applications for Buildings-Specifications*, ISO 22762-3:2010.

Japan Electric Association (JEA) (2000), *Design and Technical Guideline of Seismic Isolation Structure for Nuclear Power Plant*, Nuclear Standard Committee of JEA, JEAG 4614-2000.

Kim, S. and Stewart, J.P. (2003), "Kinematic soil structure interaction from strong motion recording", *J. Geotech. Geoenviron. Eng.*, ASCE, **129**, 323-335.

Lee, N.H. and Song, K.B. (1999), "Seismic capacity evaluation of the prestressed/reinforced concrete containment, Young-Gwang nuclear power plant units 5 & 6", *Nucl. Eng. Des.*, **192**, 189-203.

Liao, S. and Zerva, A. (2006), "Physically-compliant, conditionally simulated spatially variable seismic ground motions for performance-based design", *Earthq. Eng. Struct. Dyn.*, **35**, 891-919.

Luco, J.E. and Wong, H.L. (1986), "Response of a rigid foundation to a spatially random ground motion", *Earthq. Eng. Struct. Dyn.*, **14**, 891-908.

Malushte, S. and Whittaker, A.S. (2005), "Survey of past base isolation applications in nuclear power plants and challenges to industry/regulatory acceptance", *Proceedings of 18th International Conference on Structural Mechanics in Reactor Technology*, SMiRT 18, Beijing, China, August.

McKenna, F. and Fenves, G.L. (2001), *OpenSees, the Open System for Earthquake Engineering Simulation*, http://opensees.berkeley.edu.

Micheli, I., Cardini, S., Colaiuda, A. and Turroni, P. (2004), "Investigation upon the dynamic structural response of a nuclear plant on aseismic isolating devices", *Nucl. Eng. Des.*, **228**, 319-343.

Mwafy, A.M., Kwon, O.S., Elnashai, A. and Hashash, Y.M.A. (2011), "Wave passage and ground motion incoherency effects on seismic response of an extended bridge", *J. Bridge Eng.*, ASCE, **16**(3), 364-374.

Nour, A., Cherfaoui, A., Gocevski, V. and Leger, P. (2012), "CANDU 6 nuclear power plant: Reactor building floor response spectra considering seismic wave incoherency", *Proceedings of the 15th World Conference of Earthquake Engineering*, Paper no. 78. Lisbon, Portugal, September.

Novak, M. and Hindy, A. (1979), "Seismic response of buried pipelines", *Proceedings of the 3rd Canadian Conference on Earthquake Engineering*, Montreal, Canada, January.

Schellenberg, A., Yang, T.Y. and Kohama, E. (2013), *OpenSees Navigator 2.5.2*, https://nees.org/resources/osnavigator.

Sobczyk, K. (1991), *Stochastic Wave Propagation*, Kluwer Academic Publishers, Netherlands.

Soneji, B.B. and Jangid, R.S. (2008), "Influence of soil-structure interaction on the response of seismically isolated cable-stayed bridge", *Soil Dyn. Earthq. Eng.*, **28**(4), 245-257.

Stewart, J.P., Conte, J.P. and Aiken, I.D. (1999), "Observed behavior of seismically isolated buildings", *J. Struct. Eng.*, ASCE, **125**(9), 955-964.

Tongaonkar, N.P. and Jangid, R.S. (2003), "Seismic response of isolated bridges with soil–structure interaction", *Soil Dyn. Earthq. Eng.*, **23**(4), 287-302.

United States Nuclear Regulatory Commission (USNRC) (2012), Standard Review Plan for the Review of Safety Analysis Reports for Nuclear power Plants, 3.7.2. Seismic System Analysis, NUREG-0800, USNRC, Washington, USA.

Vanmarcke, E.H., Fenton, G.A. and Heredia-Zavoni, E. (1999), *Conditioned Earthquake Ground Motion Simulator*, SMIQKE-II User's manual, Version 2.1.

Vanmarcke, E.H., Heredia-Zavoni, E. and Fenton, G.A. (2003), "Conditional simulation of spatially correlated earthquake ground motion", *J. Eng. Mech.*, ASCE, **119**(11), 2333-2352.

Zerva, A. (1993), "Pipeline response to directionally and spatially correlated seismic ground motions", *J. Press. Ves. Tech.*, ASME, **15**, 53-58.

Zerva, A. (2009), *Spatial Variation of Seismic Ground Motions: Modeling and Engineering Applications*, Taylor & Francis Group, CRC Press, Florida, USA.

Zerva, A. and Zervas, V. (2002), "Spatial variation of seismic ground motions: An overview", *Appl. Mech. Rev.*, **55**(3), 271-297.

Zhao, C. and Chen, J. (2013), "Numerical simulation and investigation of the base isolated NPPC building under three-directional seismic loading", *J. Nucl. Eng. Des.*, **265**, 484-496.

CC